

Sharp pair spectra and excited states of rare-gas impurities in metals*

R. A. Tilton, D. J. Phelps, and C. P. Flynn

Department of Physics and Materials Research Laboratory, University of Illinois, Urbana, Illinois 61801

(Received 24 February 1975)

Optical-absorption spectra in the photon energy range 6–11.5 eV are reported and interpreted for Kr and Xe impurities present at various concentrations in random rare-gas–alkali-metal alloys. The Xe spectra show structure at energies more than 2.5 eV above threshold, even in dilute alloys. This is interpreted as arising from *d*-like excited states, and provides evidence that the electron gas near impurities can be excited into a variety of persistent configurations. Sharp symmetrical absorption lines ~ 200 meV wide that emerge with increasing impurity concentration in both Kr and Xe alloys are shown to originate from pairs of rare-gas atoms. The sharpness of these pair lines and the general form of the spectra are interpreted in terms of specific ground and excited configurations closely related to states of diatomic rare-gas molecules. Similar results are also presented for heteroatomic Xe-Ar pairs.

I. INTRODUCTION

Much information concerning the electronic and vibrational structure of impurity multiplets in insulators has been derived from optical measurements that probe the excitation spectrum, symmetry, and so forth of the impurity-host complex. For metals the investigation of impurity structure has advanced largely by means of other, frequently less penetrating techniques, mainly because the mobile conduction-electron gas makes most metals opaque in the energy range of interest for valence excitations.^{1,2} Nevertheless, a large body of information concerning the structure of isolated impurities has emerged from resistivity, susceptibility, NMR and other techniques.¹ Evidence for impurity pairing and complex formation has also accumulated, principally from measurements of mechanical properties and in particular from studies of anelasticity.³ X-ray investigations have also revealed the short-range order parameters,⁴ and hence the interaction energies between impurities, in metallic alloys. However, these methods generally lack the power of optical techniques.

Since impurity valence electrons usually mix into the host conduction-band^{1,5} impurity-induced changes of the optical spectrum at photon energies through the range 0–1 Ry of electron-hole pair creation processes mainly contain information concerning the deformation of band states caused by the impurity. It has been realized recently that impurities in metals have configurations accessible to valence excitations quite different from these band electron-hole pair states.⁶ The essential difference is that the hole may trap at the impurity. Since the impurity must remain electrically neutral it follows that an extra electron must also localize there, leaving the impurity much like an excited atom. The description of rare-gas excitations in

alkali metals presented in the preceding paper⁷ (referred to as I) provides a first clear-cut example of this behavior for simple valence impurities. Existing results⁸ for transition-metal impurities may require similar atomlike interpretations, as also do core hole spectra in which the holes are effectively trapped on one lattice site,⁹ and perhaps even slowly moving holes in the *d* bands of pure transition metals. The spectroscopy of these *locally* excited configurations offers an impurity chemistry in metals whose study is hardly begun.

The present paper is devoted mainly to a new aspect of this field: the study of the excitation spectra of impurity *pairs* in metals. It is shown in what follows that impurity pairing effects modify in a radical way the excitation spectra of rare-gas atoms in metals. Sharp excitation lines ~ 200 meV wide emerge, contrary to the normal expectations for metallic hosts. These effects will be explained in terms of a particular novel excited-state structure of rare-gas pairs in alkali-metal host lattices.¹⁰ There also exists evidence suggesting that rare-gas atoms can sustain a variety of excited states in which the electron gas persists in different configurations after the excitation process is complete.

II. APPARATUS

The equipment used for the optical measurements reported here was precisely that described in Paper I, and no recapitulation is necessary. Samples were deposited, as before, onto LiF substrates at liquid-He temperatures, and the ratio of the transmitted light intensities through the alloy and pure metal samples was directly obtained. In one respect, the present procedures differed significantly from those described in Paper I. In early efforts to grow samples con-

taining both Xe and Kr impurities, it was not found possible to control the sample compositions by leaking rare-gas mixtures through a common capillary nozzle. A different procedure was required to achieve the necessary precision. This finding is somewhat disturbing as other groups in similar investigations have employed capillary tubes or leak valves to introduce rare-gas mixtures into the sample preparation chamber. It therefore seems possible that the rare-gas concentrations were not accurately determined in these earlier studies.

It is well known that capillary leaks¹¹ can operate in a regime intermediate between laminar and Knudsen flow and thus have flow rates which are complicated functions of the driving pressures. For this reason, the flow of gas mixtures across capillary leaks is particularly hard to predict, and, for a mixture, it cannot be expected that the proportion of two gases passed through a capillary leak be independent of the driving pressure or the capillary diameter. In our own system, a further difficulty arose. The leads from the two gas bottles, together with the leads to the Wallace-Tiernan gauge, produced substantial mixing times (i.e., times required to obtain a homogeneous mixture of the two gases).

To eliminate these difficulties, a system was constructed in which the two gases flowed separately through independent capillary leaks into a common tube leading to the sample preparation chamber. The two capillary leaks were calibrated separately using a quartz crystal as before, and then calibrated when operating together. In the latter case, the mass deposited per second onto the crystal was found to be precisely the sum of the fluxes for the two capillary tubes taken separately. This result is to be expected since the presence of a second gas at low pressure near the outlet of a capillary nozzle is negligible compared to the pressure gradient across the capillary. The benefits of this system were immediately reflected in the reproducibility and systematization of the optical spectra, and no difficulties traceable to the twin capillary systems were encountered at any subsequent time. A consequence of these techniques is that we are able to present *absolute* optical-absorption data and so discuss the absolute oscillator strengths even in these complex systems. It is shown in Sec. IV that these results provide a significant insight into the excitation spectra of heteroatomic rare-gas pairs.

III. RESULTS

Figure 1 presents the absorption profiles for Xe in potassium for various Xe concentrations in

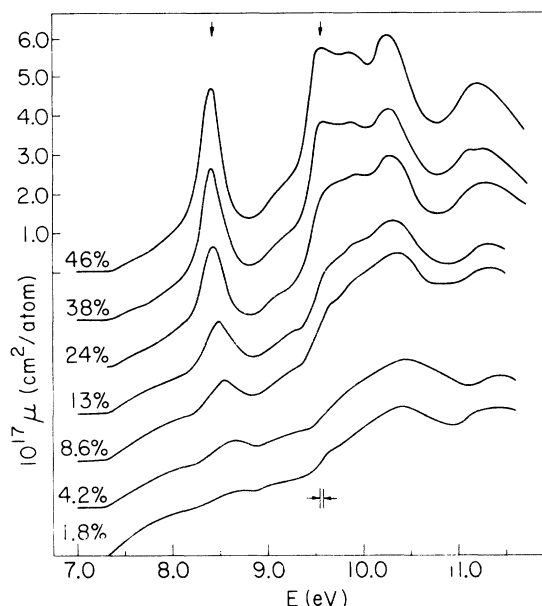


FIG. 1. Absorption per Xe atom at 7°K for Xe impurities at various concentrations (at.%) in potassium.

the range 0–50 at.%. Note that *absolute* absorption coefficients are indicated. The sample preparation was tightly controlled, and the data can therefore be presented in the form of absorption cross sections per impurity atom. Similar, but less extensive data are presented for Xe in Rb and Xe in Cs in Figs. 2 and 3. We shall comment here on some particular features of these results before passing on to the description of other impurity-host systems. The Xe-K system has been most fully studied and the detailed comments that follow are restricted to this one example.

Neither the threshold energy E_t at which absorption begins, nor the threshold profile above E_t ,

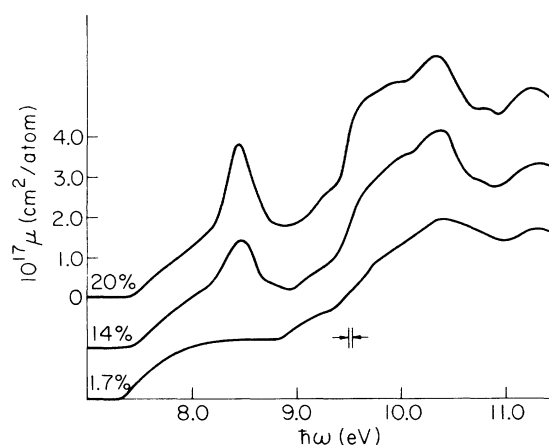


FIG. 2. Absorption per Xe atom at 7°K for Xe impurities at various concentrations (at.%) in rubidium.

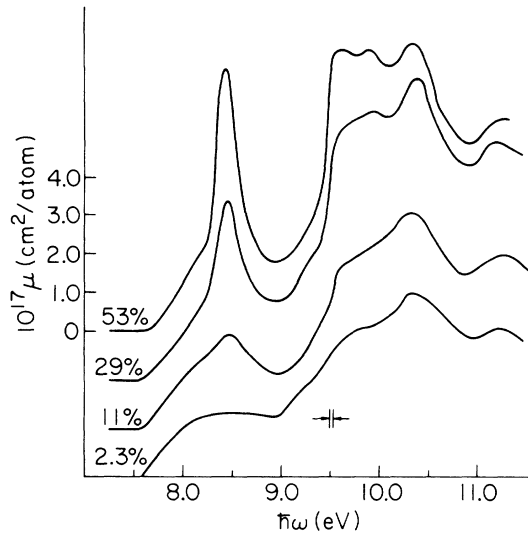


FIG. 3. Absorption per Xe atom at 7°K for Xe impurities at various concentrations (at.%) in cesium.

remain independent of sample composition in XeK alloys. Figure 4(a) shows how the threshold shifts to higher energies as the Xe concentration increases. The shift is not large (~ 0.1 eV); it grows most rapidly in the Xe concentration range $0 < c_{\text{Xe}} < 12$ at.%. At the same time the profile changes in an apparently simple manner. When fitted to a form $f(E) = A(E - E_t)^{-\alpha}$ (see Paper I), the coefficient α remains constant at a value $\alpha = -0.9 \pm 0.1$ within the stated uncertainty. The reduced absorption at higher c then follows almost entirely from the change of A with composition. Figure 4(b) shows how A varies almost linearly with c_{Xe} , although within substantial uncertainties. In order to indicate the trend we have drawn a broken line through the data, extrapolating to $A = 0$ at $c = 100$ -at.% Xe. This trend is, of course, highly suggestive of a metal-induced threshold profile, in corroboration of the discussion in Paper I.

The sharp peaks that emerge with increasing impurity concentration in Figs. 1–3 provide some of the most interesting and important results of this work. It is shown in Sec. IV that they arise from pairs of rare-gas atoms that lie at neighboring sites in the lattice. The peaks do not fall at fixed energies but, rather, their positions depend somewhat on impurity concentration. Figure 4(c) gives the location of the first peak in XeK alloys as a function of Xe concentration. It may be remarked that the bulk of the shift occurs at low impurity concentrations and takes the peak to lower energies. A substantial part of this shift may arise from a deformation of the profile caused by the spin-orbit replica of the threshold.

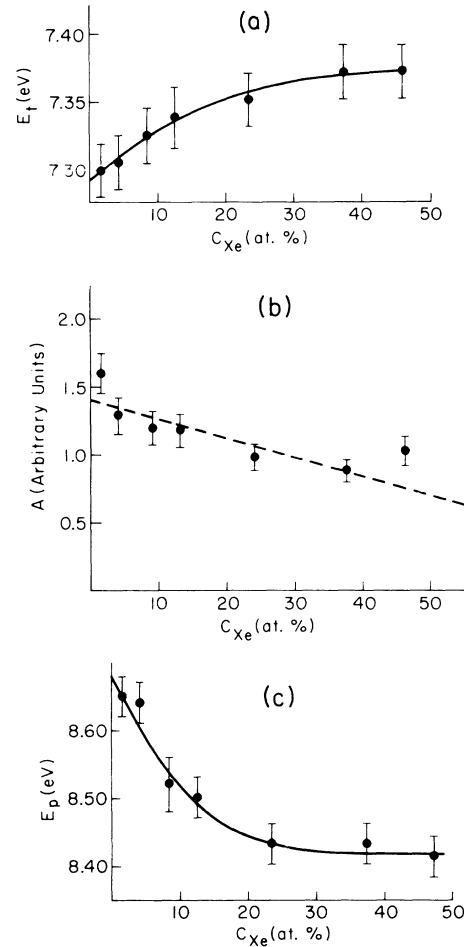


FIG. 4. Concentration dependence of the Xe spectrum in potassium: (a) threshold energy, E_t ; (b) threshold constant A ; (c) energy of the lowest pair peak.

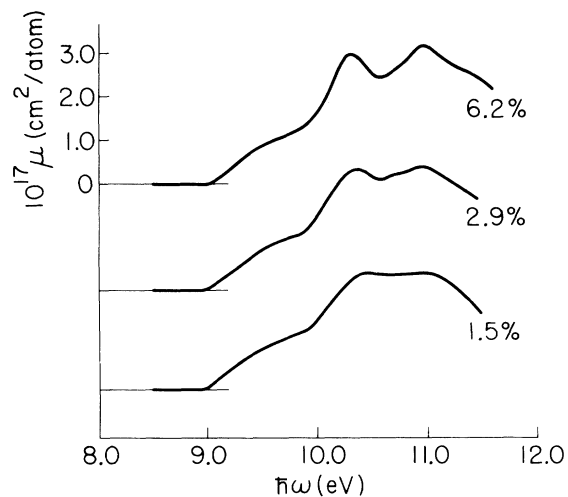


FIG. 5. Absorption per Kr atom at 7°K for Kr impurities at various concentrations (at.%) in potassium.

The threshold profile and its spin-orbit replica underlay the pair peak in these spectra.

Results for Kr impurities in relatively dilute K, Rb, and Cs alloys are presented in Figs. 5, 6, and 7. The spectra have a simpler appearance than those of Figs. 1-3 because the accessible energy range of absorption was limited by the LiF cutoff, so that absorption associated with d -like final states was not observable. First, as for Xe impurities, the Kr spectra change significantly with impurity concentration. Most interesting among those trends is the emergence of sharp peaks with increasing impurity concentration. These peaks shift with composition much as in the case of XeK displayed above (Fig. 4). The KrRb system has been studied across the full phase diagram, in combination with resistivity measurements that reveal the metal-insulator transition. These data will be found in Paper III.¹² Results showing the variation of threshold energy with composition are also presented there. The trends are similar to those observed for XeK alloys. It may be remarked, however, that the threshold coefficient A in KrRb was not found to undergo changes identical with those shown in Fig. 4 for XeK. A difficulty for Kr impurities is that the first pair peak falls closer to the threshold energy than in XeK. As the threshold energy increases and the peak energy decreases, with increasing Kr concentration, the tail of the peak begins to overlap significantly with the threshold profile and makes the analysis uncertain. Thus, we cannot judge with certainty whether or not the XeK results of Fig. 4(c) are, in this respect, typical of all rare gases in alkali metals.

Of the wide range of available rare-gas-alkali-metal alloys, most effort was expended on Xe and Ar impurities in the K host. Potassium was

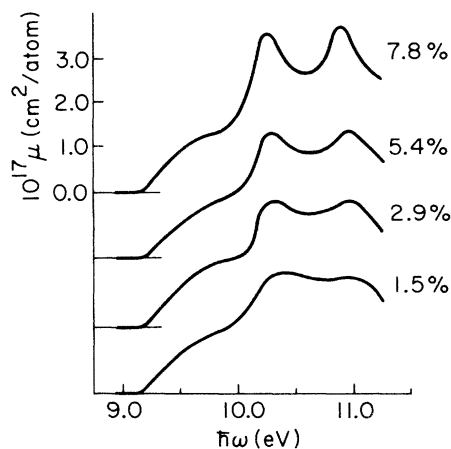


FIG. 6. Absorption per Kr atom at 7°K for Kr impurities at various concentrations (at.%) in rubidium.

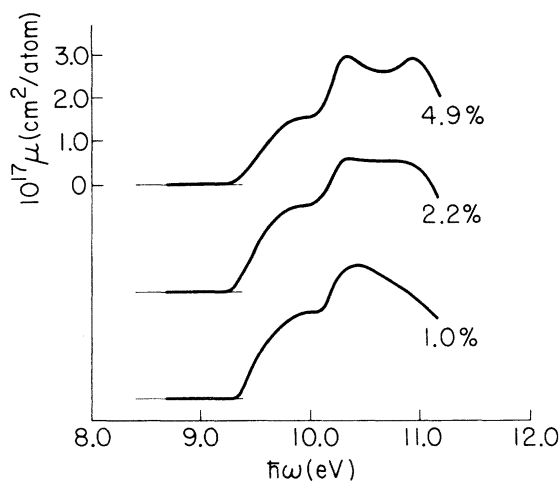


FIG. 7. Absorption per Kr atom at 7°K for Kr impurities at various concentrations (at.%) in cesium.

chosen since it has both a small impurity misfit and a plasma energy sufficiently below the impurity excitations that its optical window wholly overlaps the accessible impurity absorption. Spurious effects due to host band excitations are thereby avoided. Xenon was chosen as the primary test species because its atomic excitation spectrum has much structure at low energies below the cutoff of the LiF substrate at $\hbar\omega \approx 12$ eV and above the strong plasma absorption by conduction electrons at $\hbar\omega \approx 5$ eV in the metal. In the initial experiments Kr was employed as a perturbation on the XeK system and results resembling those described below were obtained. An unavoidable complexity arose, however, from the strong overlap of the Kr and Xe absorption spectra. In order to avoid this difficulty, Ar, rather than Kr, was employed in the final studies because the excitation threshold for isolated Ar atoms was expected to occur at higher energies (~ 11 eV).

Since the interactions between rare-gas species is unnecessarily complex in alloys involving high densities of both rare gases, we chose to investigate the effects of Ar on low densities of Xe impurities. In this way, spectra from Xe₂ pairs were largely avoided (see e.g., Fig. 1 for Xe₂ spectra in K). Moreover, Ar₂ spectra fall at energies (~ 11 eV) near the LiF cutoff and, consequently, are not fully accessible to this study. Thus Ar-Xe interactions can be expected to dominate the spectrum for Ar concentrations large compared to the Xe concentration. In order to secure both a good signal-to-noise ratio and a small total impurity content, densities of 2 and 4 at.% were chosen for the Xe test species, and Ar concentrations in the range of 0-15 at.% were chosen in order to span the fixed Xe concentra-

tions in a satisfactory way.

The results of these experiments are shown in Figs. 8 and 9. In Fig. 8 are displayed the absolute absorption coefficient per Xe atom (the logarithm of the ratio of transmitted light intensities normalized to the density per unit area of Xe atoms in the alloy) at 7 K for rare-gas impurities in XeArK alloys containing about 2-at.% Xe and 0–15-at.% Ar. The samples were not annealed, so segregation and ordering of the impurities is largely avoided. Similar results are shown in Fig. 9 for alloys containing about 4-at.% Xe, and Ar concentrations up to 16 at.%. These spectra reveal a wealth of details including a pronounced shift in the Xe threshold, the emergence of the Ar threshold, and a marked change in the integrated oscillator strength within the accessible energy range.

IV. DISCUSSION

Notable among the Kr data of Figs. 5–7 is the apparent growth, with increasing impurity concentration, of sharp absorption peaks superposed on a threshold profile that is rather insensitive to composition in the more dilute systems. For Kr impurities these remain the only marked features of the results because the LiF cutoff has limited our studies to photon energies less than about 11.5 eV. For Xe impurities, however, some structure remains visible on the absorption curves

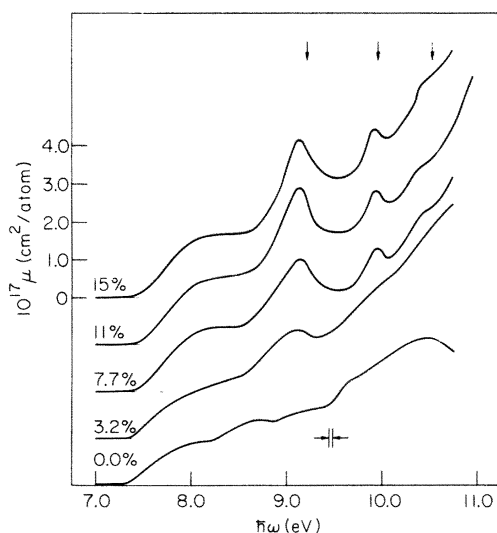


FIG. 8. Optical absorption per Xe atom in thin potassium films containing about 2-at.% Xe, showing how the absorption changes with various additions of Ar.

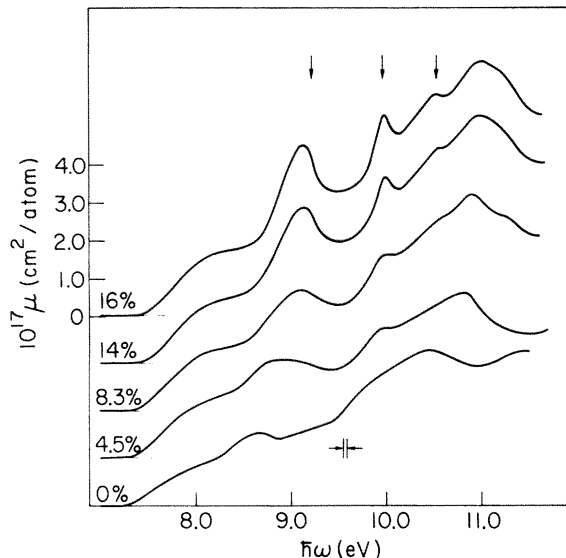


FIG. 9. Optical absorption per Xe atom in thin potassium films containing about 4-at.% Xe, showing how the absorption changes with various additions of Ar.

at energies greater than 2 eV above threshold, even for the dilute alloys.

These features are treated separately in the following discussion. The threshold absorption in dilute systems has been examined fully in Paper I. Section IV A discusses the observed sharp peaks in order to identify their properties and origins. An interpretation of these properties in terms of specific impurity structures follows in Sec. IV B. Finally, Sec. IV C analyzes the structured absorption that occurs more than 2.5 eV above threshold in dilute alloys containing Xe.

A. Pair peaks and threshold profiles

It is clear from the spectra presented in Sec. III, and particularly for the more detailed XeK results of Fig. 1, that the sharp peaks on the absorption curves grow smoothly with increasing impurity concentration. The form of this functional dependence on composition provides the basis from which the present analysis proceeds.

Figure 10 shows the height of the 8.4-eV peak in Fig. 1 plotted as a function of Xe impurity concentration. Clearly, the peak height grows linearly with Xe content. This linear variation appears to show unambiguously that the excitations originate on rare-gas atom pairs, since only the probability that a second impurity occupies any specific site neighboring the test atom changes linearly with concentration in truly random alloys. Fur-

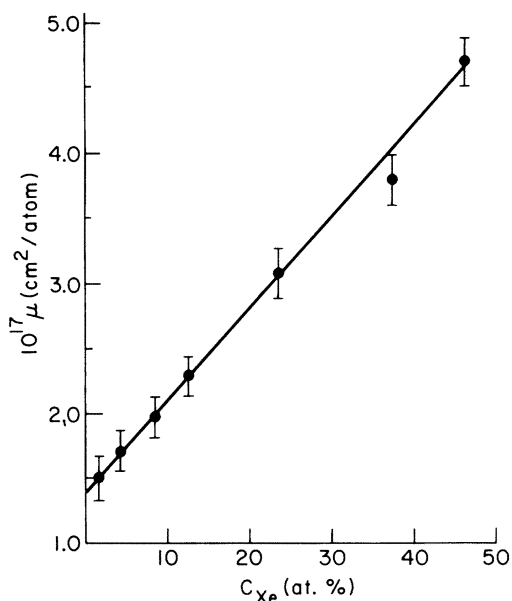


FIG. 10. Absorption coefficient at the 8.4-eV pair peak for Xe in K, shown as a function of xenon concentration.

thermore, since screening is essentially completed inside the Wigner-Seitz cell of metallic hosts,^{5,13} there can be very little long-range interaction among impurities. Therefore the interacting atoms in each pair are almost certainly in close proximity. Leaving until Paper III an explicit demonstration that the samples are characterized by random short-range order, we conclude that the sharp spectral lines originate from pairs of rare-gas atoms occupying nearest-neighboring sites in the metallic host lattice.

Data taken on rather dilute alloys (e.g., the Kr data of Figs 5–7) are not, in general, suitable for this type of analysis. The absorption curves are not sufficiently precise for small fractional changes in absolute amplitude of the absorption to show clearly in figures depicting the amplitude as a function of concentration. An additional ambiguity arises in that the positions of some sharp peaks shift with composition. This happens in part because other components of the absorption occupy the same energy interval. To exhibit the broad trend of peak behavior a different approach was therefore adopted. The smooth trend of absorption above and below the 8.4-eV peak was interpolated under the peak itself and the peak height taken as the maximum amplitude $\delta\mu$ of the observed absorption above the interpolated background. It should be noted that no obvious changes of peak width with composition were detected, so the measured $\delta\mu$ provide an approximate, but

satisfactory, measure of the oscillator strength in the peaks.

The results of this analysis are shown in Fig. 11 for Kr impurities and Fig. 12 for Xe impurities. The substantial scatter present in the data, particularly for the dilute systems, reflects the uncertainty present both in the data and in the crude method adopted for the analysis. Nevertheless, the results agree quite well with the trend established in Fig. 8 for XeK. The Kr results for alloys with $c < 10$ at.% all conform in a satisfactory way to a linear dependence of $\delta\mu$ on c . Even more interesting is the fact that the Xe results yield linear plots of $\delta\mu$ against c out to quite large Xe concentrations. Data taken on Kr impurities at higher impurity concentrations were found to maintain the linear trend also. It is shown in what follows that this behavior corresponds to the existence of an independent excitation channel for the impurity pairs.

Consider first the *isolated* pairs. In a lattice for which each point has N nearest neighbors, the probability that one impurity, with atomic fraction c , has one nearest-neighbor impurity, and that the pair has no other nearest impurity neighbors, is

$$P_2 \sim c(1-c)^{N+N'-1},$$

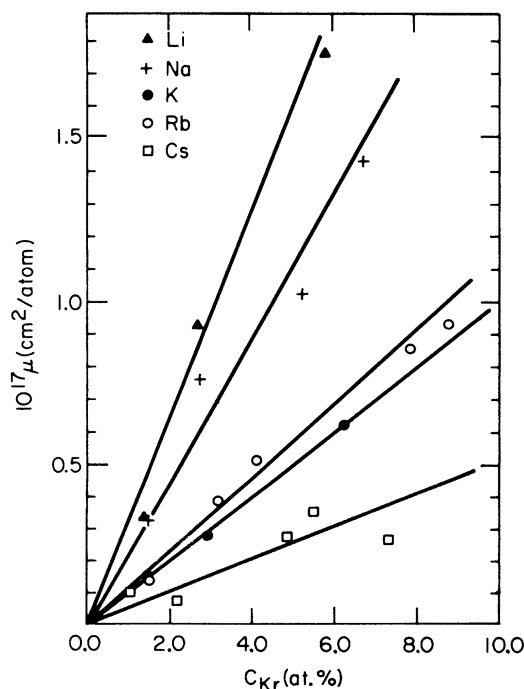


FIG. 11. Height $\delta\mu$ of the pair peak as a function of Kr impurity concentration in various alkali-metal-Kr solutions.

with $N+N'$ the total number of nearest neighbors possessed by the pair. Here $Nc(1-c)^{N-1}$ is the probability that any impurity has one and one only nearest impurity neighbor, and the factor $(1-c)^{N'}$ eliminates assemblies in which the neighbor has other impurity neighbors. For the bcc lattice $N=8$ and $N'=7$ so that

$$P_2 \sim 8c(1-c)^{14}.$$

P_2 is shown as a function c in Fig. 13. Clearly the probability of finding *isolated* pairs deviates markedly, at higher impurity concentrations, from the linear trend it follows up to $c \sim 2$ at.%. Since the pair peak amplitudes shown in Figs. 7-9 remain linear to much larger impurity concentrations it can be inferred that the observed features do *not* arise from excitations of impurities located in isolated impurity pairs. In order that $\delta\mu$ remains linear in c out to such large concentrations, it is necessary instead that *all* nearest-neighboring impurity atoms each contribute an increment to the pair peak absorption, *regardless of the types of atoms that occupy sites neighboring the pair*. The number P'_2 of such pairs to which any test atom belongs is just $P'_2 = Nc$. This varies linearly over the entire composition range, and the experimental results find a natural explanation.

Thus, the observed concentration dependence shows that the pair peaks arise from pair *bonds*¹⁰ between impurities, rather than from isolated pairs alone. There is also a strong indication that the observed spectra are influenced largely by very short-ranged couplings in the alloys.

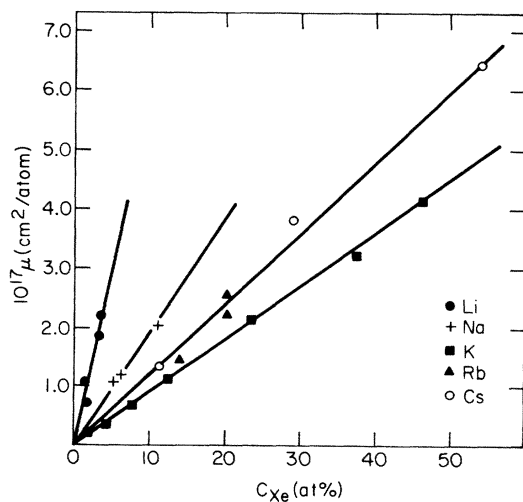


FIG. 12. Height $\delta\mu$ of the pair peak as a function of Xe impurity concentration in various alkali-metal-Xe solutions.

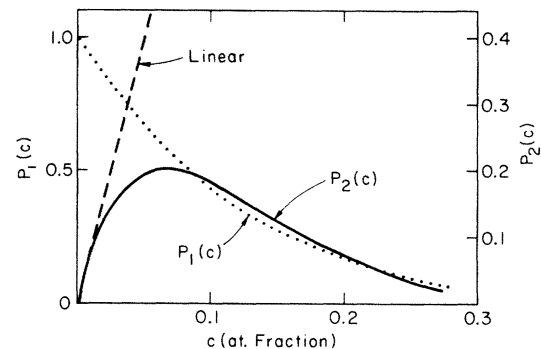


FIG. 13. Probabilities for impurities to be in various complexes. The solid line shows the probability $P_2(c)$ that an impurity is one member of an *isolated* pair and the dotted line represents the probability P_1 that it is an *isolated* single impurity. The broken, linear extrapolation of $P_2(c)$ indicates the number of pair bonds per impurity.

A second feature of the results leads to a similar conclusion and adds some insight into the couplings that influence the excitation spectra. In Paper I we have identified the absorption near threshold with the excitation of *isolated* impurity atoms, and the identification is confirmed beyond doubt by our ability to predict the threshold energy with high precision. But the results for more concentrated samples presented in Sec. III show that the threshold persists up to very high impurity concentrations, at which few impurities lack impurity neighbors. This follows from the probability

$$P_1 \sim (1-c)^N \sim (1-c)^8,$$

that an impurity at concentration c shall be isolated from other impurities in a bcc lattice having the components distributed at random among lattice sites. P_1 is shown as a function of c by the broken line in Fig. 11. It falls off essentially to zero for $c \sim 0.25$. Since the threshold absorption persists well beyond this impurity concentration it seems quite certain that impurity atoms having other impurities as neighbors must also contribute to the absorption in the energy region immediately above the observed threshold. In fact the particular linear decay of threshold profile with c exhibited by Xe in K [Fig. 4(b)] suggests that the oscillator strength falls in direct proportion to the number of nonmetallic neighbors possessed by the impurities, so that the pair peak and the threshold profile *both* reflect the densities of various types of pair bonds connecting to impurities in the alloys. This conclusion cannot, however, be maintained with certainty for the case of threshold processes owing to the complications caused by threshold shifts and problems of analysis men-

tioned in Sec. II.

In contrast to the situation for homoatomic pairs as discussed above, the spectral changes with increasing Ar concentrations, displayed in Figs. 8 and 9, are so severe that the relation to spectra from samples lacking Ar is largely obliterated. As mentioned in Sec. III, the alloy components and compositions were so chosen that the results would pertain mainly to the properties of XeAr pairs located on neighboring sites. This point is confirmed by the three sharp peaks which emerge with increasing Ar concentration in both the 2- and 4-at.% Xe alloy series. To analyze these features we have estimated the peak heights by interpolating the background into the region under the peaks using the trends from both higher and lower energies. This procedure provides only an approximate description of the oscillator strength in each peak, but, since the peak shapes seem relatively insensitive to other variables, it does provide a serviceable method of dealing with the variation of oscillator strength with impurity content.

In Fig. 14, the peak heights, *not* normalized to unit Xe concentration, are presented as function of the product, $c_{\text{Xe}}c_{\text{Ar}}$, of the Xe and Ar atomic fractions. The data for each of the peaks fall in a satisfactory way on one of the three lines in Fig.

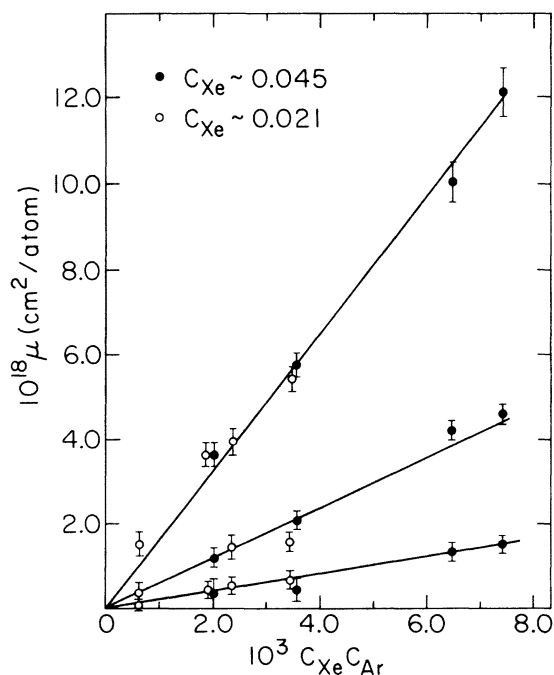


FIG. 14. Heights of the sharp peaks in Figs. 8 and 9, shown as functions of the product $c_{\text{Ar}}c_{\text{Xe}}$.

14. The form of this functional dependence on concentration associates the lines unambiguously with pairs consisting of one Xe atom and one Ar atom occupying neighboring sites in the host lattice. But, just as in the case of homoatomic pairs, the linearity extends up to Ar concentrations that are too large for these features to arise from *isolated* pairs. In the most concentrated alloys, the total rare-gas concentration rises to 20 at.%, and few if any isolated pairs remain. We therefore deduce, as before, that the sharp peaks arise from pair *bonds* between Xe impurities and neighboring Ar impurities.

Another feature of the sharp pair spectra also emerges in Figs. 8 and 9. The Xe_2 pair peak at about 8.6 eV is clearly visible in spectra with $c_{\text{Ar}}=0$ but disappears as Ar is added to the alloy and in the limit of large Ar concentrations is totally lacking. In the intermediate range (e.g., the sample containing 4-at.% Xe and 4-at.% Ar) a broadened peak, spreading between the energy of the Xe_2 peak at $c_{\text{Ar}}=0$ and the first XeAr peak at $c_{\text{Ar}} \gg c_{\text{Xe}}$, is observed. Similar results have been observed in rare-gas alloys lacking a metallic component.¹⁴ It seems that Ar neighbors drain oscillator strength from the Xe_2 excitations into transitions ending on final XeAr states, since the density of Xe_2 pair bonds is presumably rather constant among the samples described by Fig. 9.

The question of integrated oscillator strength is an important aspect of the results discussed here and in Paper I. Note that these experiments measure transmissivity rather than absorption and thus are subject to the uncertainty of reflection losses from the samples, which consist of successive layers of Ne, metal (or alloy), and LiF. However, the data represent only differences between pure metal and alloy samples. Also, the reflectivity losses in these dilute alloys remain small and may not modify the data in a critical way. The systematic variation of measured oscillator strength with composition then follows with reasonable fidelity the behavior of the true oscillator strengths for the impurity transitions. We therefore evaluate for the various alloys, the quantity

$$g(E_m) = \int_{E_t}^{E_m} \mu(E) E dE,$$

with μ the measured absorption coefficient, to determine the oscillator strength integrated from threshold to a fixed upper limit E_m .

In Fig. 15(b), the values of $g(E_m)$ for alloys containing 2-at.% Xe are displayed as open circles, and those for alloys with 4-at.% Xe as closed circles.

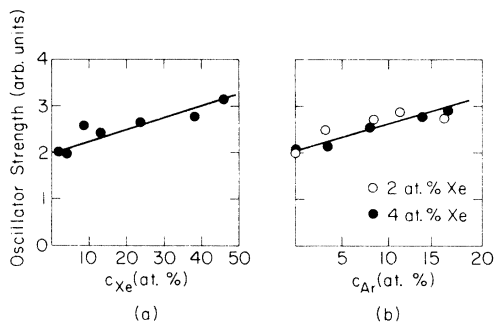


FIG. 15. Oscillator strength per Xe atom (a) in K-Xe mixtures and (b) in K-Xe mixtures with additions of Ar.

cles. In each case the value $E_m = 10.5$ eV was chosen in order to avoid substantial contributions from the Ar threshold absorption. From Fig. 4(b), one deduces that the Ar neighbors cause a substantial increase in the oscillator strength of Xe atoms in the energy range below 10.5 eV. The same straight line provides a good approximation to the data from both the 2- and 4-at.% Xe alloys, and it may therefore be presumed that this line accurately describes these alloys in the dilute Xe limit. If extrapolated to $c_{Ar} = 100$ at.%, these results suggest that the oscillator strength per Xe atom in this energy range is increased by a factor of 3 to 4 by the presence of a complete shell of Ar atoms. This large factor may well measure in part the suppression of the impurity oscillator strength by the electron gas in the dilute impurity limit. A similar analysis for Xe atoms in K, derived from the results shown in Fig. 1 is displayed in Fig. 15(a), which shows integrated oscillator strength per Xe atom below 10.5 eV plotted against c_{Xe} . Once again the trend is linear, although the Xe oscillator strength seems less sensitive to the presence of Xe neighbors than to presence of Ar neighbors, and the extrapolated enhancement at $c_{Xe} = 100$ at.% is only a factor ~ 2 .

Much of the added oscillator strength in XeK and XeArK systems lies in the sharply peaked rare-gas absorption which is evidently to be associated with pair bonds between rare-gas atoms. We must therefore conclude that the pair excitations provide a low-energy outlet for oscillator strength that, for isolated rare-gas impurities, is forced to higher energies by the constraint of the host electron gas. This, of course, is the expected result of the Anderson orthogonality catastrophe (see Paper I).

B. Excited configurations of rare-gas impurities

In this section we interpret the observed excitation spectra in terms of specific ground and excited state structures, making use of the view-

points established in Sec. IV A. The concentration dependence of the threshold and pair peak data discussed there establishes profiles characteristic of the dilute limit. These were associated in Paper I with rare-gas impurities isolated in the metal lattice. The ground state of the isolated impurity appears much like a rare-gas atom occupying a relaxed vacant cell of the metal, and the excited state resembles a perfect alkali-metal lattice slightly distorted by the ground-state relaxation. The conduction electron densities in and near the defect cell are sketched in Figs. 16(a) and 16(b) for the ground and excited configurations, respectively. The impurity potential binds a full valence shell of six p electrons far below the band in Fig. 16(a) and five p electrons are bound still deeper in the defect cell of Fig. 12(b). We recall here that the identification of these configurations is supported by the precision with which the threshold may be predicted. Although the profile above threshold clearly arises from electron-hole pair creation in the alkali-metal-like excited configuration, the form of this profile cannot as yet be predicted by the theory.

The results show that the threshold absorption persists, somewhat shifted and reduced in amplitude, when other rare-gas atoms occupy sites neighboring the excited atom. Our first purpose in what follows is to identify the excited configurations that cause this threshold absorption at higher concentrations. The discussion centers on the excited states possessed by *pairs* of

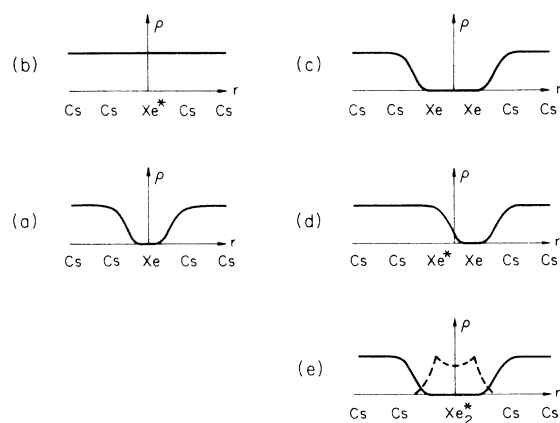


FIG. 16. Electron density $\rho(r)$ near (a) the one-impurity ground state; (b) the one-impurity excited state; (c) the two-impurity ground state; (d) the two-impurity "metallic" excited state; and (e) the molecular excited state responsible for the pair peaks. The figure is drawn for Xe in Cs but the structures are probably insensitive to the particular host and impurity species.

neighboring rare-gas atoms, but it should be realized throughout that the states identified are probably insensitive to the presence of a limited number of other rare-gas atoms neighboring the pair.

The electron density in the ground configuration of two rare-gas atoms occupying neighboring sites in an alkali metal is shown schematically in Fig. 16(c). The valence p shells of the rare-gas atoms fall ~ 1 Ry below vacuum level and cannot mix with the alkali conduction bands which lie at $E > -0.5$ Ry. In order to secure local electrical neutrality the electron gas is repelled from the two vacant cells. For this reason the structure closely resembles two rare-gas atoms occupying the two cells of a relaxed divacancy. The relaxation around each component impurity should not differ widely from that for an isolated rare-gas atom in the lattice.

It is expected from the persistence of threshold absorption to high impurity concentrations that the excited states of homoatomic rare-gas multiplets causing this effect bear a strong resemblance to single-impurity excited configuration of Fig. 16(b). The threshold for this new process must fall close to that for Fig. 16(b) and the coupling to electron-hole pair creation processes must also be similar, in order that the profile shall remain insensitive to composition for $c \lesssim 10$ at. % of impurity. Figure 16(d) shows the only likely candidate for the threshold process. In this excited configuration the excited atom resembles a host alkali atom and the excitation process merely fills in one component impurity cell with electron gas. As far as the electron gas is concerned, the excitation merely annihilates one vacancy much as in the excitation leading from Fig. 16(a) to 16(b). Further support for this assignment will be found in the discussion of heteroatomic excitations presented below. It remains possible that the hole and its conduction-electron screen could hop between the two degenerate impurities of a homoatomic pair, but the lack of overlap between the electron gas configurations in the two orientations must inhibit this process. It is likely that the system traps in one or the other orientation for its limited lifetime. Further comments on this point will accompany our subsequent discussion of the pair peaks.

In order to explain the data, the transition 16(c) \rightarrow 16(d) must have its threshold at only slightly higher energy (~ 0.1 eV) than the process 16(a) \rightarrow 16(b). It is easily shown that the two processes do indeed fall in very similar energy ranges. Neglecting relaxation interactions between the defect cells one sees that the excited configura-

tion 16(d) differs from 16(b) only in the presence of one extra relaxed impurity cell whose formation energy is approximately that (~ 0.2 eV) required to form a vacancy. Similarly, 16(c) differs from 16(a) by the presence of one *extra* relaxed impurity cell, but the two impurities now lie on adjacent lattice sites. The energy of the ground state is thus lowered further than that of the excited state by the nearest-neighbor binding energy of the impurities. This interaction must closely resemble the vacancy-vacancy binding which is ~ 0.1 eV in alkali metals.¹⁵ Thus, the excitation energy is increased only slightly, probably ~ 0.1 eV, by the presence of a second impurity on a site neighboring the excited atom. This is precisely the threshold behavior required to explain the observed profiles.

It is more difficult to argue convincingly that the trend of observed *profiles* with concentration fits equally well with the model excited configuration of Fig. 16(d). In the absence of a theory describing the profile for the excitation 16(a) \rightarrow 16(b), it is hard to predict the further changes induced by a perturbation. One may nevertheless observe that the coupling may, to some extent, reflect the degree of overlap between the excited atomic orbital and the surrounding electron gas. The coupling of the transition to the host valence states may thus decrease in proportion to the fraction of neighboring sites occupied by other rare-gas atoms. Certainly, this is the inference to be drawn (albeit tentatively) from the data presented in Fig. 4(b), but neither the experiment nor the interpretation have as yet identified this feature with certainty.

Consider now the pair peaks. It follows from Sec. IVA that these processes are associated with pair *bonds* between impurity rare-gas atoms. However, the extraordinary sharpness of the excitations is unexpected for metallic host lattice. In fact, the widths and locations of the lines resemble the recombination lifetime-limited exciton lines of these atoms when condensed as solid rare gases (for details see Paper IV).¹⁶ Evidently the metallic features of the surrounding host have little influence on the pair peak profiles. Thus, the data seem to involve novel structures on whose excitation spectrum the influence of electron-hole creation processes is negligible.

The latter feature provides a strong indication that rare-gas pairs (or multiplets) dispersed in a metallic host possess at least two independent excitation channels. This follows from the fact that a channel strongly coupled to pair-creation processes can hardly exhibit sharp structure. This seems to rule out the possibility that excitations leading to Fig. 16(d) are so modified from 16(b) by

the presence of a second neighbor that a sharp absorption peak emerges from the electron-hole pair creation spectrum some distance above threshold. Instead, these unusual effects must arise from the availability of an independent excitation channel.

An excited configuration that explains the position, sharpness, and pair-bond nature of the observed pair peaks is shown in Fig. 16(e). It is a symmetrical configuration that centers equally on two impurity atoms involved in the excitation. For this reason the observed dependence of the oscillator strength on the density of impurity pairs follows trivially. The p hole in the full valence shells of the two rare-gas atoms resonates between the two systems while the excited s -like orbital also encompasses both centers. In short, the pair peaks arise from an excited configuration of the diatomic rare-gas molecule.

A further point warrants immediate mention in connection with the pair peak amplitudes. Although the peak height varies linearly with the number of impurity pair bonds in the several alkali-metal hosts, the strength of this dependence is sensitive to the particular host employed. It seems likely that the fractional oscillator strength residing in the pair peak depends on the hopping rate of the one-electron excitation between the components of the impurity pair. The dependence on the internuclear separation thus implied suggests that the rapid emergence of the pair peaks with composition observed in the lighter alkali metals may arise from the smaller lattice spacing of these hosts, as the smaller lattice parameter forces the impurities into closer proximity.

Matters related to the location of the pair peaks are deferred until the discussion in Paper IV of the principal resonance lines of diatomic and more complex systems formed from both like and unlike rare-gas species. The present discussion is concerned with the fact that configuration 16(e) offers a convincing explanation of the unusual sharpness exhibited by both the Xe and Kr pair peaks in all the alkali-metal hosts.¹⁷ It is well known that a reduced overlap associated, for example, with increasing atomic separation, must eventually cause an electron gas to become magnetic. This happens because overlap determines the hopping rate and, for sufficiently slow translational motion, the exchange interaction eventually becomes dominant. For local phenomena these processes manifest themselves in the magnetism associated with the rather sharp d orbitals of many transition metals in simple metals having relatively dilute electron gases. The magnetism is low when, as in the case of Mn in Al, the electron gas is dense and the overlap becomes too large.¹⁸

Its spread through two unoccupied cells evidently allows the excited orbital in 16(e) to reduce its overlap with the electron gas below the level of overlap in states 16(b) and 16(d). We believe that the exchange then predominates and the excited orbital exists as a spin polarized state of the system. Whether the orbital is degenerate with the host band states, or falls below the band bottom as a bound state, then has little effect on the sharpness of the excitation spectrum. In either case the excitations are lifetime-broadened δ functions.

A detailed demonstration of this result is deferred until Paper V (Ref. 16) but the reasons are sufficiently simple that a physical explanation will suffice here. A full magnetic level appears in the theory of impurity structure as a virtual bound state in which the phase shift having the appropriate symmetry passes from 0 to π in the energy range of the relevant orbital.^{1,18} But a phase shift of π does not change the asymptotic form of band wave functions; it corresponds only to a multiplicative factor of -1 . For this reason a local excitation whose only effect is to introduce a full virtual level causes no long-range changes in the distribution of conduction electrons, and the electron-hole pair creation processes associated with such changes are completely eliminated. The excitation spectrum thus becomes a δ function broadened only by lifetime limitations on the excited state.

It may be remarked that fully bound excited states also lack substantial coupling to pair creation processes. Of course, the distinction between bound and virtual levels is sharp only in one-electron theory.¹⁹ Nevertheless, the lack of coupling between conduction electrons at E_F and full local valence levels remains a reality in the complete many-body system. It finds its most obvious expression in the lack of residual resistance associated, for example, with the d levels of Mn when dispersed in noble-metal hosts.²⁰ It seems likely that the magnetic excited states of rare-gas pairs do, in fact, contribute a virtual level to the electron gas since the binding energy of the excited molecular orbital probably falls close in energy to the analogous atomic s orbital, and is therefore degenerate with the band states of alkali-metal hosts. A bound-to-virtual transition of this orbital should, however, have little influence on the excitation spectrum.

In summary, the excited state 16(b) of isolated rare-gas impurities exerts a dominant influence on the observed excitation spectra only in the dilute limit with $c \lesssim 5$ -at.% rare gas. The apparent persistence of the threshold absorption, and of the general low-energy impurity profile,

is observed only because excitations 16(d) of rare-gas pairs (and multiplets) give spectra similar to those for 16(b). The observed threshold shift to higher energies conforms both in sign and order of magnitude with the theoretical expectations, and the change in profile can be explained in a plausible, but as yet incomplete, way. The sharp lines of the spectra arise from molecular excitations of rare-gas pairs (or multiplets), and the excited orbital in these configurations probably forms a virtual-bound state in the host conduction band.

Turning now to the spectra for alloys containing heteroatomic pairs we note that the results shown in Figs. 8 and 9 contain information concerning two distinct thresholds. As $c_{\text{Ar}} \rightarrow 0$, the threshold absorption of Xe at dilution in K is obtained in accordance with Fig. 1. The addition of Ar shifts this absorption to higher energies and appears to blur the threshold into a smoothly rounded form. A marked increase in the amplitude of this "metallic" absorption is also clearly evident in Figs. 8 and 9. The influence of Ar neighbors on Xe absorption is quite marked.

In addition to these interesting changes in the Xe threshold profile, the presence of Ar atoms gives rise to a new absorption feature at high energies. Clearly evident in the XeArK spectrum as $c_{\text{Ar}} \rightarrow 0$ is a maximum in the optical density at $\hbar\omega \approx 10.5$ eV (cf. also Fig. 1.). This peak is completely obscured in Figs. 8 and 9 by additional absorption at $\hbar\omega \geq 10.5$ eV. In what follows, we interpret this new absorption as originating in "metallic" type excitations centered on Ar impurities.

It is easy to estimate the absorption threshold of Ar atoms in K, using the methods of Paper I. The formation energy of unrelaxed vacancies in K is about 0.6 eV and, neglecting relaxation, this value represents the increase of the ground state energy when Ar is introduced into the K host. Since Ar^* resembles K, the energy of the impurity excited state is lowered by 0.94 eV, the cohesive energy of K. The Ar atomic transition at 11.62 eV is thus reduced in energy by the metallic environment to produce a threshold at $11.62 - 0.94 - 0.6 \approx 10.1$ eV, neglecting strain effects. For the cases of Kr in Rb and Xe in Cs, relaxation in the ground and excited states shifts the absorption threshold upward by ~ 0.5 eV (see Fig. 9 of Paper I). Much the same shift should occur for Ar impurities in K, so that the final prediction is an absorption threshold of 10.6 eV for Ar impurities in K, with an expected precision of ± 0.1 eV. This prediction is in excellent agreement with the observed absorption just above 10.5 eV which earlier comments have associated with Ar impurities in

XeArK alloys.

The behavior of the threshold and pair peaks in XeArK mirror similar features in alloys containing one rare-gas species. All the available evidence is consistent with the absence of short-range ordering in these alloys. Therefore the low-energy impurity spectra from dilute XeK alloys containing ~ 10 -at.% Ar represent mainly the spectrum of XeAr pairs, since each Xe has, on the average, one Ar neighbor and no Xe neighbors. The similarity between the spectra of alloys containing 2- and 4-at.% Xe confirms that the dilute Xe limit is indeed being probed. There are now two principal points to be established in confirmation of the model developed above to describe the excited state structure. These points relate, respectively, to the threshold absorption and the pair peaks.

The data for alloys containing Xe and Ar impurities give clear evidence that impurity pairs support asymmetric excitations in which the host electron gas propagates mainly through one excited impurity cell and not its neighbor. The point is that a Xe-like metallic threshold with substantially unmodified oscillator strength persists in alloys containing Ar concentrations (~ 10 at.%) for which most Xe atoms must neighbor Ar impurities. A separate Ar absorption threshold is also observed. These results demonstrate that each atom of the impurity pair can be excited almost as if the other were absent, although with some distortion of the absorption profile. The shift of the Xe threshold to higher energies, which accompanies increasing Ar concentration, is a natural consequence of the interaction of the Xe atom with its Ar neighbor through the lattice strain and the Van der Waal's attraction.

The second point concerns the sharp peaks which are identified above with transitions ending on homoatomic rare-gas molecules. The association

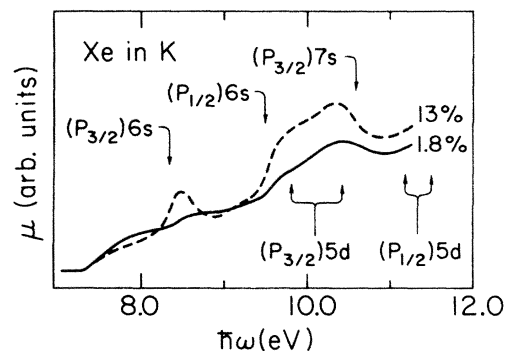


FIG. 17. Absorption coefficient of Xe in K at two concentrations, showing the coincidence of sharp structure with atomic Xe transitions marked by arrows.

of these features with interactions between two rare-gas species is strongly supported by the linear dependence of the peak height on $c_{\text{Xe}}c_{\text{Ar}}$ exhibited in Fig. 14. The persistence of the linearity at large c_{Ar} further confirms that the excitation involves pair *bonds* rather than merely isolated XeAr pairs. Furthermore, the fact that XeAr associates yield a spectrum of sharp excitations radically different from that of Xe_2 pairs suggests that the excitation encompasses *both* atoms of the impurity pair. These peaks must therefore originate in transitions ending on states which are truly molecular in nature.

C. *d*-like absorption

A residual structure appears at energies more than 2.4 eV above threshold for the Xe excitations even in dilute alloys. As in the case of the threshold profiles, this structure reproduces in general form from one host lattice to the next, but the energies at which various broad features emerge appear less sensitive to the particular embedding lattice than is the case for the threshold energy. We believe that this structure relates to a new feature of excited impurity configurations in metals: the existence of a variety of alternative electron gas configurations near a local center in a metal. This possibility has mainly been neglected in previous studies of local optical excitations in metals.²¹

In any discussion of excited states far above threshold in metals two different possibilities must be recognized. For the sake of definiteness we shall use here the example of rare-gas excitations in metals, but it should be emphasized that these remarks have a more general validity. First, it is possible that the excited configurations above threshold resemble the threshold excitation 16(b) with added quasiparticles propagating through the alkali-metal valence levels. This is the alternative to which discussions in the current literature largely conform. The second alternative, which we believe also occurs in the systems of interest here, is that optical absorption may excite a *different* self-consistent distribution of conduction electrons in and near the defect cell. In the present studies it is an orbital of *d* symmetry that is excited from the full ground-state *p* shell. The *d* excitation has its own threshold, and excitation of still higher energy in part presumably create this electron gas configuration together with electron-hole pairs in the new self-consistent set of excited band orbitals which locates a *d* state in the central cell.

We shall comment further here only on the experimental justification for these beliefs. In Fig. 17 are superposed the absorption curves of Xe in K at 1.8% and 13% concentrations, for the purpose of comparison with the spectrum of *gaseous* Xe, indicated in Fig. 17 by arrows. The lower pair peak falls near the $5p^6 \rightarrow 5p^56s$ ($J = \frac{3}{2}$) atomic resonance and its $J = \frac{1}{2}$ partner forms the lower edge of the absorption structure extending from about 9.6 to 10.7 eV in the metal. The high-energy portion of this range coincides with strongly allowed $5p^6 \rightarrow 5p^55d$ transitions of atomic Xe. Similar features in the spectrum of pure solid Xe are discussed in Paper IV. In what follows it is shown that the latter part of the absorption attributed to Xe in the metal has an evolution with impurity concentration different from that exhibited by the pair peaks. It must therefore be identified with a separate excited configuration most probably possessing a local *d*-like symmetry.

For the present purpose the most interesting point is that the *d* structure is not eliminated by decreasing the impurity concentration. To measure this effect we have determined the height $\delta\mu_d$ by which absorption at ~ 10.1 eV in Fig. 1 exceeds the linear interpolation between the trough at ~ 10.9 eV and the point at ~ 9.1 eV at which the upper pair peak begins to modify the absorption (see Fig. 17). The resulting value of $\delta\mu_d$ is shown as a function of c in Fig. 18. The point established by these results is that the *d*-like structure persists in the extrapolation of the results down to zero impurity concentration.

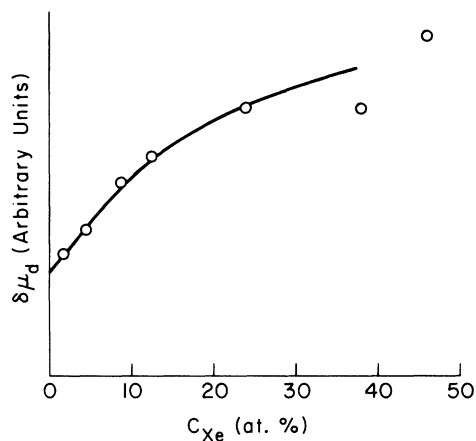


FIG. 18. Amplitude $\delta\mu_d$ (see text) of *d*-like absorption by Xe at various concentrations in potassium. This component does not vanish as $c \rightarrow 0$, thereby identifying a new basic excited state of isolated Xe impurities in the metal host.

As a result of these observations we conclude that the electron gas near impurity centers in metals can exist in more than one form for lifetimes exceeding 10^{-15} sec. The plasma energy exceeds the width of the observed structures by a substantial factor. It therefore follows that these excited configurations are self-consistent structures. The configurations therefore persist in the usual way by means of Coulomb correlations among particles in the electron gas. This latter observation follows from the fact that one-electron lifetimes of conduction electron-impurity collisions

must surely be less than $\sim 10^{-15}$ sec, corresponding to the conduction electron bandwidth, as is certainly the case for the excited configuration 16(b). One anticipates that excitations related to successively higher atomic states will eventually have lifetimes shorter than the conduction-electron-impurity collision lifetime so that the notion of a self-consistent configuration loses its meaning. Nevertheless, the results discussed here point clearly towards a future spectroscopy of low-lying self-consistent excited configurations of the electron gas near impurities in metals.

*Research supported in part by the NSF under Grant No. DMR-7203026.

¹For references in specific areas, see C. P. Flynn, *Point Defects and Diffusion* (Oxford U.P., Oxford, 1972).

²Optical properties of metals and alloys are reviewed by P. O. Nilsen, *Solid State Physics*, edited by F. Seitz, D. Turnbull, and H. Ehrenreich (Academic, New York, 1974), Vol. 29; see also, *Optical Properties and Electronic Structure of Metals and Alloys*, edited by F. Abeles (North-Holland, Amsterdam, 1965).

³For reviews, see A. S. Nowick and R. W. Heller, *Adv. Phys.* **12**, 251 (1963); **14**, 101 (1965); **16**, 1 (1967). Interstitial pairing is discussed by R. F. Mattas, Thesis, (University of Illinois, 1974) (unpublished); R. F. Mattas and H. Birnbaum, *Acta Met.* (to be published).

⁴See, for example, S. C. Moss and P. C. Clapp, *Phys. Rev.* **171**, 764 (1968); and the review by G. Fournet, in *Phase Stability in Metals and Alloys* (McGraw-Hill, New York, 1967).

⁵J. Friedel, *Adv. Phys.* **3**, 446 (1954). Many papers in the area of impurity structure in metals are gathered in *J. Phys. Radium* **23**, 594 (1962).

⁶J. J. Peters and C. P. Flynn, *Phys. Rev. B* **6**, 3343 (1972).

⁷D. J. Phelps, R. A. Tilton, and C. P. Flynn, preceding paper, *Phys. Rev. B* **14**, 5254 (1976).

⁸See, for example, A. B. Callendar and S. E. Schnatterly, *Phys. Rev. B* **7**, 4385 (1973); H. P. Meyers, L. Wallden, and A. Karlson, *Philos. Mag.* **8**, 725 (1968); C. O.

Norriss and P. O. Nilsen, *Solid State Commun.* **6**, 649 (1968); and other work discussed in Ref. 2.

⁹For references in this rapidly expanding area see the reviews by F. C. Brown and by G. D. Mahan, in *Solid State Physics*, edited by F. Seitz, D. Turnbull, and H. Ehrenreich (Academic, New York, 1974), Vol. 29.

¹⁰R. A. Tilton and C. P. Flynn, *Phys. Rev. Lett.* **34**, 20 (1975).

¹¹See, e.g., S. A. Gordon, *Rev. Sci. Instrum.* **29**, 501 (1958).

¹²D. J. Phelps and C. P. Flynn, following paper, *Phys. Rev. B* **14**, 5279 (1976).

¹³N. F. Mott, *Proc. Cambridge Philos. Soc.* **32**, 281 (1936); J. S. Langer and S. H. Vosko, *J. Phys. Chem. Solids* **12**, 196 (1959).

¹⁴G. Baldini, *Phys. Rev.* **128**, 1562 (1962).

¹⁵There exist no firm values for this quantity but a rough estimate would be one third of the vacancy formation energy, as in the case of noble metals: C. G. Wang, D. N. Seidman, and R. W. Bulluffi, *Phys. Rev.* **169**, 553 (1968).

¹⁶R. A. Tilton and C. P. Flynn, second following paper, *Phys. Rev. B* **14**, 5289 (1976).

¹⁷C. P. Flynn, third following paper, *Phys. Rev. B* **14**, 5294 (1976).

¹⁸See J. Friedel, *Can. J. Phys.* **34**, 1190 (1956); and *J. Phys. Radium* **23**, 692 (1962).

¹⁹N. F. Mott, *J. Phys. Radium* **23**, 594 (1962).

²⁰C. R. Vassel, *J. Phys. Chem. Solids* **7**, 90 (1958).

²¹See, however, Ref. 6.